Ni/CaO-Al_2O_3 Bifunctional Catalysts for Sorption-Enhanced Steam Methane Reforming

Pan Xu, Zhiming Zhou, Changjun Zhao, and Zhenmin Cheng
State Key Laboratory of Chemical Engineering, East China University of Science and Technology, Shanghai 200237, China

DOI 10.1002/aic.14543
Published online July 5, 2014 in Wiley Online Library (wileyonlinelibrary.com)

Ni/CaO-Al_2O_3 bifunctional catalysts with different CaO/Al_2O_3 mass ratios were prepared by a sol–gel method and applied to the sorption-enhanced steam methane reforming (SESMR) process. The catalysts consisted mainly of Ni, CaO and $Ca_5Al_6O_{14}$. The catalyst structure depended strongly on the CaO/Al_2O_3 mass ratio, which in turn affected the CO_2 capture capacity and the catalytic performance. The catalyst with a CaO/Al_2O_3 mass ratio of 6 or 8 possessed the highest surface area, the smallest Ni particle size, and the most uniform distribution of Ni, CaO, and $Ca_5Al_6O_{14}$. During 50 consecutive SESMR cycles at a steam/methane molar ratio of 2, the thermodynamic equilibrium was achieved using the catalyst with a CaO/Al_2O_3 mass ratio of 6, and H_2 concentration profiles for all the 50 cycles almost overlapped, indicating excellent activity and stability of the catalyst. Moreover, a high CO_2 capture capacity of 0.44 g_{CO_2}/g_{cat} was maintained after 50 carbonation–calcination cycles, being almost equal to its initial capacity (0.45 g_{CO_2}/g_{cat}).
 AIChE J, 60: 3547–3556, 2014
Keywords: sorption-enhanced steam methane reforming, bifunctional catalyst, hydrogen, structure-property relationship, stability

Introduction

It is well known that CO_2 as a greenhouse gas contributes significantly to anthropogenically forced climate change.[1] The CO_2 emissions come mainly from combustion of fossil fuels for power generation, transportation, manufacturing industries (such as steel and cement), and various chemical processes.[2] In recent years, although biomass-based fuels and clean energy such as hydroelectric, wind, solar, and nuclear energy have gained much attention, fossil fuels will continue to be the dominant source in the foreseeable future.[3] With this respect, reduction of fossil fuel-derived CO_2 emissions is of great importance.[2,3]

Conversely, H_2 as a clean energy carrier has a great potential to lower CO_2 emissions.[4] At present, steam methane reforming (SMR) is the most widely used technology for H_2 production in industry, and typically involves the use of a steam reformer, high- and low-temperature water–gas shift reactors and some purification units for CO_2 removal. However, the reversible and strongly endothermic feature of the reforming reaction requires severe reaction conditions and a number of units with low overall efficiency.[5,6] Introduction of *in situ* CO_2 capture into SMR, that is, the so-called sorption-enhanced SMR (SESMR), appears to be a promising technology to replace the conventional SMR. Compared to the SMR, the SESMR has many advantages, such as increased conversion of CH_4 and high-purity H_2, decreased reaction temperature, simplified proce
ss and reduced capital cost, and improved energy efficiency.[7,8] In addition and more importantly, if CaO is used as the sorbent for CO_2 removal in the SESMR, regeneration of saturated sorbent normally produces high-purity CO_2 suitable for use or sequestration,[9–12] which also contributes to reduction of CO_2 emissions.

Most investigations on the SESMR process are conducted using individual catalyst and sorbent particles, that is, catalyst and sorbent (two different particles) are physically mixed and then loaded into a reactor.[13–21] CaO is the most commonly employed sorbent due to its low cost, wide availability, high CO_2 capture capacity, and high carbonation rate.[22–24] However, bulk CaO and limestone are readily subject to a significant loss in capacity after several carbonation–calcination cycles, which restricts the application of CaO to the SESMR. Many techniques are thus developed to improve the sintering-resistance performance of CaO-based sorbents, as summarized by recent reviews.[9,10,25–29]

The aim of this work is to prepare high-performance bifunctional catalysts for the SESMR process rather than individual CaO-based sorbents or Ni-based catalysts. A bifunctional catalyst that integrates catalytic and sorption properties into one particle benefits from reduced mass transfer limitations, which have been proved by theoretical studies.[30–36] Some experimental investigations are also devoted to preparing bifunctional catalysts for the SESMR. For example, Satrio et al.,[37,38] prepared core-in-shell pellets consisting of a lime or dolomite core and an alumina shell in

Additional Supporting Information may be found in the online version of this article.

Correspondence concerning this article should be addressed to Z. M. Zhou at zmzhou@ecust.edu.cn.

which a nickel catalyst was loaded. These catalysts showed increased CH_4 conversion and higher H_2 yield but poor stability over 10 cycles. Martavaltzi and Lemonidou[39] developed Ni-CaO-$Ca_{12}Al_{14}O_{33}$ catalysts by impregnating $Ni(NO_3)_2$ and $Al(NO_3)_3$ on CaO. Although higher hydrogen content (90% instead of 77% in SMR equilibrium) was obtained, the conversion of CH_4 was lower (80 vs. 95% in SMR equilibrium). In addition, only one cycle was performed. Chanburanasiri et al.[40] manufactured Ni/CaO catalysts by incipient wetness technique, and the effect of Ni loading was studied. Nevertheless, the stability of catalyst was not tested. A Ni-Ca-based catalyst derived from a hydrotalcite-like precursor was recently prepared by Broda et al.[41] via a coprecipitation technique, which yielded high-purity H_2 at 823 K and 0.1 MPa with a H_2O/CH_4 molar ratio of 4. Unfortunately, the low CaO content (21 wt %) in the catalyst led to a short prebreakthrough period. Very recently, Kim et al.[42] prepared Ni-CaO-$Ca_{12}Al_{14}O_{33}$ catalysts by combination of precipitation and hydration, and the best catalyst was found to be stable during four cycles. However, a longer test is needed to evaluate the catalyst stability. Our literature survey[37–42] suggests that the major challenge facing bifunctional catalysts today is the stability of catalyst during multiple SESMR cycles.

In this work, a sol–gel method was developed to prepare Ni/CaO-Al_2O_3 bifunctional catalysts with high activity and stability for the SESMR. The structural properties of fresh and used catalysts were characterized on the one hand, and the reactivity and stability of catalyst were tested on the other hand. Unlike previous studies, the stability of screened Ni/CaO-Al_2O_3 catalyst was further evaluated at a low but meaningful steam/methane molar ratio of 2 over 50 SESMR cycles. Moreover, the structure-property relationship of catalyst was thoroughly explored, which could guide the rational design of promising bifunctional catalysts for the SESMR process.

Experimental Section

Catalyst preparation

All the catalysts were prepared by a sol–gel method, and nickel nitrate hexahydrate, calcium lactate pentahydrate and aluminum isopropoxide were used as nickel, calcium and aluminum precursors, respectively. The mass fraction of Ni in each catalyst was maintained at 15 wt %. In a typical synthesis, 1.70 g of finely ground aluminum isopropoxide was added into 30 mL of distilled water (molar ratio of H_2O to Al^{3+} of 200:1), and then the mixture was heated by an oil bath to 358 K and hydrolyzed under reflux for 1.5 h at a stirring speed of 500 rpm. Next, the pH value of the solution was adjusted to about 3 using acetic acid, and the temperature was increased to 368 K for 10 h of hydrolysis-condensation reactions, after which 1.11 g of nickel nitrate hexahydrate, 4.66 g of calcium lactate pentahydrate, and 20 mL of distilled water were added, and the mixture solution was allowed to stir for another 6 h. Finally, the formed gel was dried in an oven at 383 K for 24 h, and the obtained hard, light green material with a smooth surface was ground into a powder, followed by calcination in a muffle furnace at 1123 K for 2 h. The as-prepared bifunctional catalyst had a theoretical CaO/Al_2O_3 mass ratio of 2, and for simplicity, this catalyst was denoted by Ni/CaAl-2. Likewise, Ni/CaAl-x represented a catalyst with a CaO/Al_2O_3 mass ratio of x which was controlled by the amounts of calcium and aluminum precursors used. For comparison, a Ni/CaO catalyst without addition of aluminum, a Ni/Al_2O_3 catalyst without addition of calcium and a CaAl-2 sorbent without addition of nickel were also prepared by the same procedure.

Catalyst characterization

The pore volume, Brunauer–Emmett–Teller surface area and average pore diameter of the catalyst were obtained by N_2 adsorption–desorption isotherms at 77 K (Micromeritics ASAP 2020), and before the measurement all samples were degassed at 423 K and 0.133 kPa for 6 h. The crystal structure of the catalyst was examined by x-ray diffraction (XRD, Rigaku D/Max 2550) with Cu Kα radiation over a 2θ range of 10–80°. The micromorphology of the catalyst was observed by a field emission scanning electron microscope (FESEM, Nova NanoSEM 450) and a high-resolution transmission electron microscope (HRTEM, JEOL JEM-2100). An energy dispersive spectrometer (EDS, EDAX Genesis XM2 system) attached to HRTEM was used for elemental analysis. The sample used for HRTEM investigation was ultrasonically dispersed in ethanol for 15 min, and then a drop of this solution was transferred onto a carbon-coated copper grid. Temperature programmed reduction (TPR, Micromeritics AutoChem 2920) was conducted using 10% H_2 in Ar with a heating rate of 10 K/min up to 1173 K, and the consumption of H_2 was monitored by a thermal conductivity detector (TCD). Chemisorption experiments used to determine the Ni dispersion of the catalyst were also performed in this apparatus. About 0.1 g of catalyst was first reduced under a flow of 30 mL/min of 10% H_2/Ar at 1073 K for 1 h using a ramp of 10 K/min, and then the reactor was purged with pure Ar at 1103 K for 1 h to remove H_2. When the sample was cooled to 308 K in Ar, H_2 pulses (0.5 mL each) were injected and the signal was monitored by the TCD. The measured H_2 uptake was used to estimate the Ni metal dispersion, assuming a H/Ni adsorption stoichiometry factor of 1.

Catalyst test

The CO_2 capture performance of bifunctional catalyst was evaluated in a thermogravimetric analyzer (TGA, WRT-3P, Shanghai Precision & Scientific Instrument), and ten consecutive carbonation–calcination cycles were carried out. About 10 mg of catalyst (150–200 μm) was placed in a platinum basket and the total gas flow rate was kept at 50 mL/min. Carbonation was conducted at 923 K for 30 min in 15% CO_2/85% N_2, and calcination at 1073 K for 10 min in pure N_2. The heating (cooling) rate was 10 K/min. The CO_2 capture capacity of a catalyst, expressed in g_{CO_2}/g_{cat}, was calculated from the weight change of the catalyst that was monitored continuously.

The SESMR experiments were performed in a fixed bed quartz reactor with an inner diameter of 16 mm. Four grams of bifunctional catalyst (150–200 μm) was loaded onto a fine-quartz fritted disk fused into the midsection of the reactor. Prior to the SESMR experiment, the catalyst was reduced *in situ* at a flow rate of 100 mL/min of 20% H_2/N_2 and the temperature program was as follows: room temperature up to 773 K at 10 K/min, then to 1073 K at 2 K/min, and finally hold at 1073 K for 1 h. Except where specified otherwise, the reforming reaction was carried out at 923 K and 0.1 MPa with a H_2O/CH_4 molar ratio of 4, and the inlet

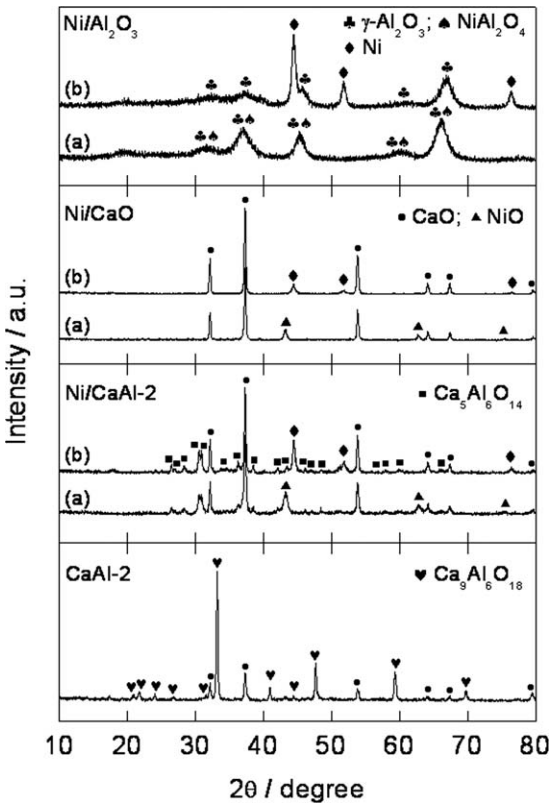

Figure 1. XRD patterns of calcined and reduced Ni/Al_2O_3, Ni/CaO, and Ni/CaAl-2 catalysts as well as the CaAl-2 sorbent: (a) calcined catalyst and (b) reduced catalyst.

flow rate of CH_4 was kept at 15.6 mL/min. Regeneration of the catalyst was conducted at 1073 K and 0.1 MPa for 1 h under a flow of 100 mL/min of 20% H_2/N_2. To compare the catalytic performance of different Ni/CaAl-*x* catalysts, 10 consecutive reforming-regeneration SESMR cycles were performed. In addition, a screened catalyst was further evaluated for 50 SESMR cycles at a low H_2O/CH_4 molar ratio of 2 to check the long-term stability of catalyst.

Results and Discussion

Physicochemical properties

The XRD patterns of calcined (without reduction) and reduced Ni/Al_2O_3, Ni/CaO, and Ni/CaAl-2 catalysts are shown in Figure 1. As a comparison, the XRD pattern of calcined CaAl-2 sorbent is also presented. The calcined Ni/Al_2O_3 exhibits diffraction peaks belonging to γ-Al_2O_3 (JCPDS 10-0425) and $NiAl_2O_4$ spinel (JCPDS 78-1601), and after reduction at 1073 K, Ni^{2+} in $NiAl_2O_4$ is reduced into metallic Ni (JCPDS 87-0712). As for Ni/CaO, the calcined sample shows lines of CaO (JCPDS 77-2010) and NiO (JCPDS 71-1179), and after reduction, the disappearance of the peaks assigned to NiO indicates the reduction of NiO into Ni. The Ni/CaAl-2 catalyst, however, displays new diffraction peaks belonging to a calcium aluminate phase $Ca_5Al_6O_{14}$ (JCPDS 70-0801), besides CaO and NiO (for the calcined sample)/Ni (for the reduced sample). $Ca_5Al_6O_{14}$ is not present in calcium and aluminum precursors, and it is, therefore, formed during preparation. The formation mechanism of $Ca_5Al_6O_{14}$ will be discussed later. In addition, an interesting phenomenon is that the CaAl-2 sorbent shows another calcium aluminate phase $Ca_9Al_6O_{18}$ (JCPDS 70-0839) instead of $Ca_5Al_6O_{14}$ in Ni/CaAl-2. The $Ca_9Al_6O_{18}$ phase was also observed for other Al-stabilized CaO-based sorbents in our recent work.[43–45] $Ca_9Al_6O_{18}$ is cubic with a unit cell of eight cyclic $Al_6O_{18}^{18-}$ anions that can be considered to be composed of six corner-sharing AlO_4 tetrahedra, while $Ca_5Al_6O_{14}$ consists of alternating sheets of distorted AlO_4 tetrahedra which are linked through corners to form a network of five-membered rings.[46] The thermal treatment is usually considered to be a factor inducing the phase transformation, as demonstrated by Mastin et al.[47] who reported the $Ca_5Al_6O_{14}$-to-$Ca_9Al_6O_{18}$ transformation after calcination of the CaO-Al_2O_3 sorbents at 1173 K. But, different calcium aluminate phases present in CaAl-2 and Ni/CaAl-2 suggest that the presence of Ni species in Ni/CaAl-2 inhibits the phase transformation from $Ca_5Al_6O_{14}$ to $Ca_9Al_6O_{18}$.

The XRD patterns of various reduced Ni/CaAl-*x* catalysts are presented in Supporting Information Figure S1. With an increase in the CaO/Al_2O_3 mass ratio, the diffraction peaks related to the $Ca_5Al_6O_{14}$ phase decrease gradually, and finally become undetectable when *x* is higher than 6, probably due to the small amount of $Ca_5Al_6O_{14}$ and its high dispersion. Conversely, the peaks assigned to the CaO phase vary slightly with *x*, and the crystallite size of CaO for various Ni/CaAl-*x* is in the range of 30.4–34.3 nm, calculated with the Scherrer equation using the CaO (200) ($2\theta = 37.4°$) peak. With regard to the metallic Ni phase in various catalysts, no remarkable difference in the peak intensity is observed.

The physical properties of various reduced Ni/CaAl-*x* catalysts are listed in Table 1. As expected, the Ni/Al_2O_3 catalyst has the highest surface area and pore volume owing to the property of the catalyst support (γ-Al_2O_3).[48,49] On adding CaO the surface area and pore volume of Ni/CaAl-*x* decrease dramatically. The CaO/Al_2O_3 ratio has a marked effect on the textural properties of Ni/CaAl-*x*. The surface area and pore volume of catalyst increase significantly when *x* increases from 2 to 6, but remain nearly the same at higher *x*. Similar to the textural properties, the dispersion of metallic Ni on Al_2O_3 is the highest (4.34%) among all the

Table 1. Physical Properties of Fresh and Used Catalysts

Catalysts	BET Surface Area (m^2/g)	Pore Volume (cm^3/g)	Average Pore Diameter (nm)	Ni Dispersion (%)
Ni/Al_2O_3	132.8	0.277	7.3	4.34
Ni/CaAl-2	11.2 (9.9)[a]	0.028 (0.093)	9.8 (38.5)	0.36
Ni/CaAl-4	17.4 (11.5)	0.058 (0.101)	12.7 (39.1)	1.10
Ni/CaAl-6	21.5 (12.1)	0.074 (0.079)	13.9 (29.0)	1.38
Ni/CaAl-8	20.1 (12.3)	0.076 (0.084)	15.3 (28.6)	1.46
Ni/CaAl-10	18.5 (10.9)	0.079 (0.086)	15.5 (22.6)	1.36
Ni/CaAl-12	18.9 (9.6)	0.083 (0.091)	15.8 (19.6)	1.42
Ni/CaO	19.3 (8.2)	0.081 (0.099)	16.6 (20.9)	1.35

[a]The data in brackets correspond to the used catalysts (after 10 SESMR cycles).

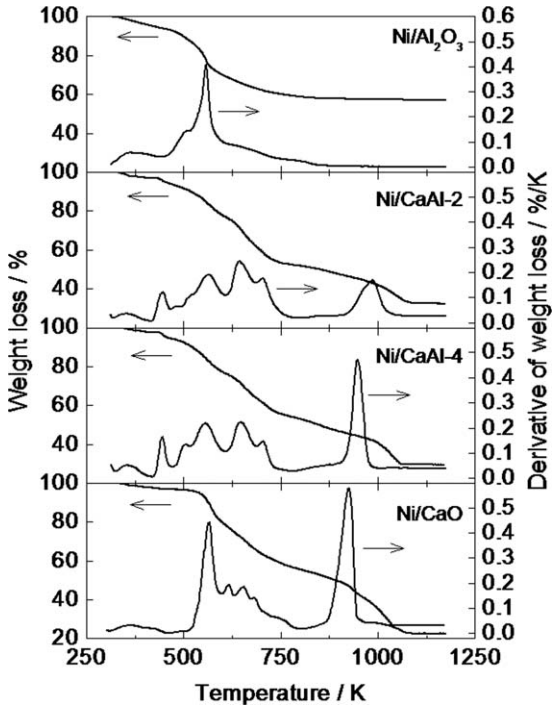

Figure 2. TG-DTG profiles of Ni/Al_2O_3, Ni/CaO, Ni/CaAl-2, and Ni/CaAl-4 precursors.

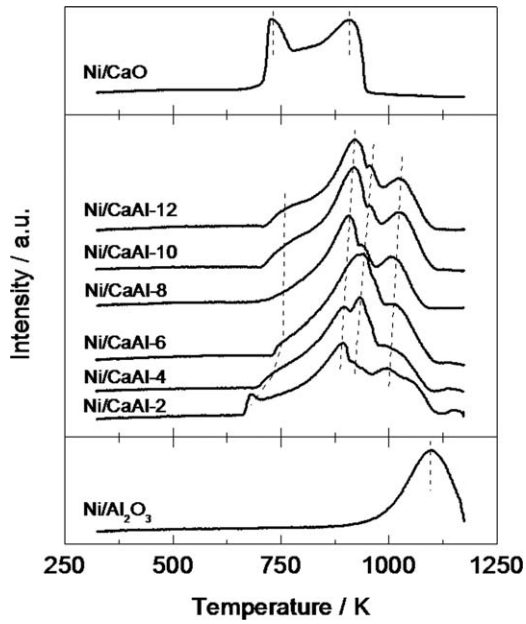

Figure 3. H_2-TPR profiles of Ni/Al_2O_3, Ni/CaO, and Ni/CaAl-*x* catalysts.

catalysts studied, and with an increase in the CaO/Al_2O_3 ratio in Ni/CaAl-*x*, the Ni dispersion first increases from 0.36% for Ni/CaAl-2 to 1.38% for Ni/CaAl-6, and then remains almost constant (about 1.4%).

The TG-DTG profiles of several catalyst precursors are shown in Figure 2, from which the formation mechanism of Ni/CaAl-*x* is explored. Three distinct peaks in the DTG profile are observed for the Ni/Al_2O_3 precursor: the first peak centered at about 373 K is ascribed to the removal of the physisorbed water, the second peak (503 K) to the release of crystal water related to $Ni(NO_3)_2$ and boehmite, and the third peak (558 K) to the decomposition of $Ni(NO_3)_2$. These peaks are also found more or less for other catalyst precursors. In addition, a broad peak centered at about 673 K for Ni/Al_2O_3 is attributed to the conversion of boehmite into γ-Al_2O_3.[50] As for Ni/CaO, besides the aforementioned peaks, the peaks between 593 and 823 K correspond to the decomposition of calcium lactate to $CaCO_3$, including the formation of some intermediate phases, and the peak at 923 K is ascribed to the decomposition of $CaCO_3$ to CaO. These peaks are also present in Ni/CaAl-2 and Ni/CaAl-4 precursors, but the intensity of the last peak decreases with decreasing CaO/Al_2O_3 ratio and meanwhile its maximum is shifted towards higher temperature, indicating that the addition of aluminum species retards the decomposition of $CaCO_3$. According to the above analyses, a possible mechanism for the formation of Ni/CaAl-*x* is proposed, as shown in Supporting Information Figure S2. The crystal water of boehmite, calcium lactate, and nickel nitrate is removed in the first step (<523 K), followed by transformation of these anhydrous species into Al_2O_3, $CaCO_3$, and NiO in the second step (523–773 K). $CaCO_3$ is further decomposed into CaO in the third step (823–1073 K), and finally, the solid-state reactions between oxides give rise to $Ca_5Al_6O_{14}$ and $NiAl_2O_4$ in the last step (1073–1123 K).[51,52] Note that a part of CaO and NiO remains even after the last step (Figure 1). $NiAl_2O_4$ is not detected in Ni/CaAl-*x* by the XRD measurement, but its presence is confirmed by the following H_2-TPR results.

Figure 3 presents the H_2-TPR profiles of various catalysts, which can be used to identify different Ni phases present in the catalyst. For Ni/CaO two distinct reduction peaks are observed. The first peak centered at 729 K is ascribed to free NiO species with a weak interaction with CaO, and the second at 908 K represents NiO species having a stronger interaction with CaO.[48] For Ni/Al_2O_3 only one peak centered at 1093 K is detected, which is assigned to $NiAl_2O_4$ spinel,[53,54] in accordance with the XRD analysis. For Ni/CaAl-*x*, however, there are four peaks (indicated by dashed lines) in the TPR patterns. The first peak is related to free NiO species, the second peak to NiO with interaction with CaO, the third peak to NiO with interaction with $Ca_5Al_6O_{14}$, and the last peak to $NiAl_2O_4$. Compared to Ni/Al_2O_3, the reduction peak of $NiAl_2O_4$ for Ni/CaAl-*x* is shifted toward lower temperature, implying that the addition of CaO into the support facilitates the reduction of Ni^{2+} in $NiAl_2O_4$. Moreover, a larger presence of free NiO is noted for Ni/CaAl-2 in comparison with other Ni/CaAl-*x* catalysts. Previous investigations have demonstrated that free NiO species normally leads to larger Ni crystallites after reduction,[54] which accounts for the lowest Ni dispersion of Ni/CaAl-2.

Figure 4 shows the FESEM images of various Ni/CaAl-*x* catalysts. It is obvious that all the catalysts possess small grains, rough surfaces, and interconnected pores, which were the desired structural characteristics of a high-performance CaO-based CO_2 sorbent.[28,29,45,55] Note that the catalysts with higher CaO/Al_2O_3 ratio, such as Ni/CaAl-12 and Ni/CaO, exhibit relatively larger grains. The HRTEM images of reduced Ni/CaAl-*x* are presented in Figure 5. It can be seen that the micromorphologies of catalyst differ from one another, depending strongly on the CaO/Al_2O_3 ratio. Ni/Al_2O_3 shows a sponge- or foam-like structure, but Ni/CaAl-2 and Ni/CaAl-4 exhibit a plate-like structure and the former has larger plates than the latter. When the CaO/Al_2O_3 ratio is above 6, the Ni/CaAl-*x* catalysts, including Ni/CaO, show a net-like structure. By combining XRD results and HRTEM

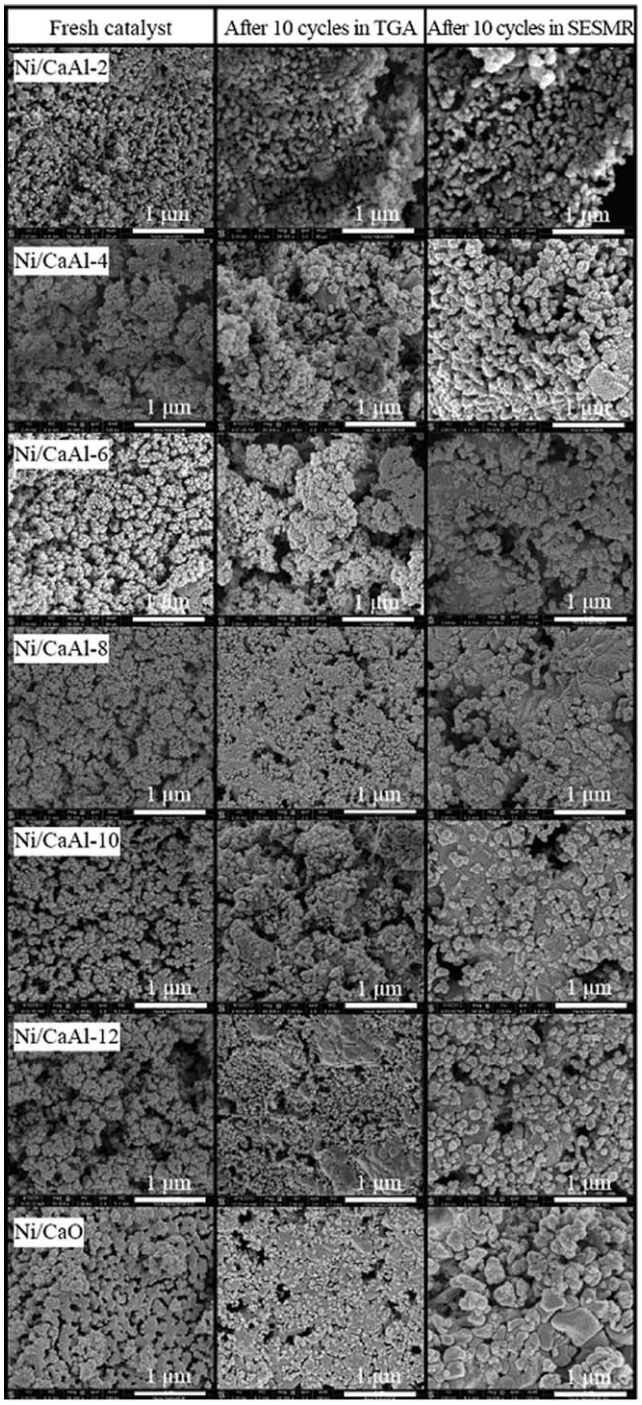

Figure 4. FESEM images of various Ni/CaAl-*x* catalysts: fresh (left column), calcined after 10 cycles in TGA (middle column), and calcined after 10 cycles in SESMR (right column).

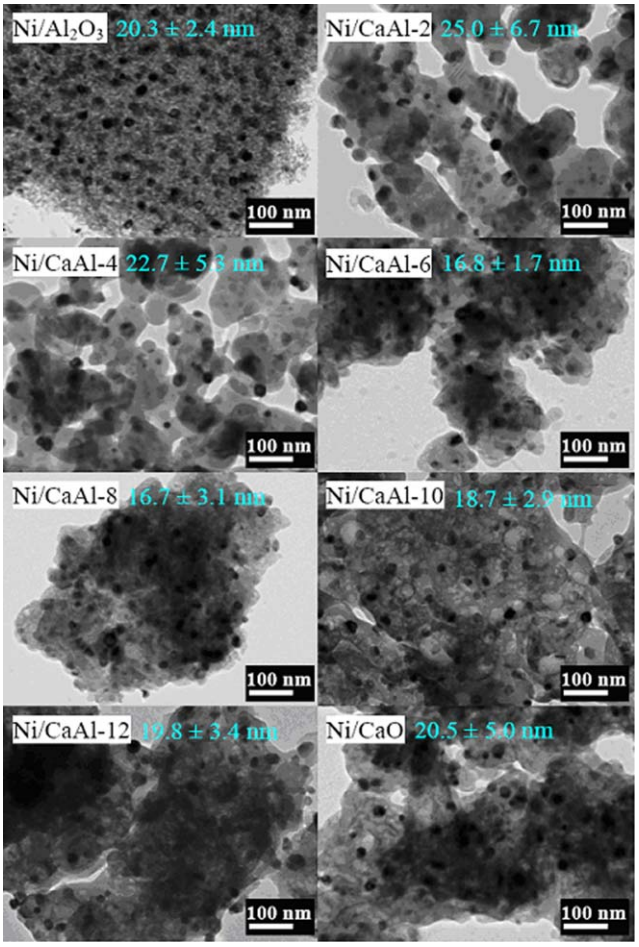

Figure 5. HRTEM images of reduced Ni/Al_2O_3, Ni/CaO, and Ni/CaAl-*x* catalysts.

[Color figure can be viewed in the online issue, which is available at wileyonlinelibrary.com.]

observations, it can be inferred that the plate-like morphology is ascribed to $Ca_5Al_6O_{14}$. This is because the dominant species in the support matrix of Ni/CaAl-2 is $Ca_5Al_6O_{14}$, whose content is much higher than that of CaO according to the amounts of Ca and Al precursors used as well as the stoichiometric calculation between CaO and Al_2O_3 to yield $Ca_5Al_6O_{14}$. The higher content of $Ca_5Al_6O_{14}$ in Ni/CaAl-2 than that in Ni/CaAl-4 explains the larger plates of Ni/CaAl-2.

For all the catalysts, the Ni particles display a quasispherical shape, and the average value of the Ni particle diameters shown in Figure 5 is calculated by $\Sigma(n_i d_i)/\Sigma n_i$, where n_i is the number of particles with a diameter of d_i. The average diameter of Ni particles first decreases from 25.0 to 16.7 nm with increasing the CaO/Al_2O_3 ratio from 2 to 8, and then increases slowly at a higher ratio, for example, 18.7 nm for Ni/CaAl-10 and 19.8 nm for Ni/CaAl-12. In particular, Ni/CaAl-2 exhibits the largest Ni particle size, which is in fair agreement with its lowest dispersion, while Ni/CaAl-6 and Ni/CaAl-8 show the smallest Ni particle size, and they also have the highest surface area (Table 1).

The element (Ni, Ca, and Al) distribution of reduced Ni/CaAl-*x* is given by the EDS mapping, as shown in Supporting Information Figure S3. The Ni/CaAl-2 catalyst clearly displays several Ca-rich areas, implying the heterogeneous distribution of CaO in the CaO-$Ca_5Al_6O_{14}$ matrix. Ni/CaAl-4 exhibits an improved distribution of CaO although the Ca-rich areas still exist. When the CaO/Al_2O_3 ratio increases to 6 or more, a uniform distribution of CaO is observed. To figure out the Ni distribution over the catalyst, Figure 6 presents individual element (Ni, Ca, and Al) maps. For Ni/CaAl-2, although Ni particles are detected over the whole catalyst, Ni-poor areas (indicated by the dashed circle) appear, and interestingly, these areas correspond to Ca-rich areas. This is mostly caused by the low Ni-Ca interaction on the one hand, and the strong interaction of Ni with Ca-Al on

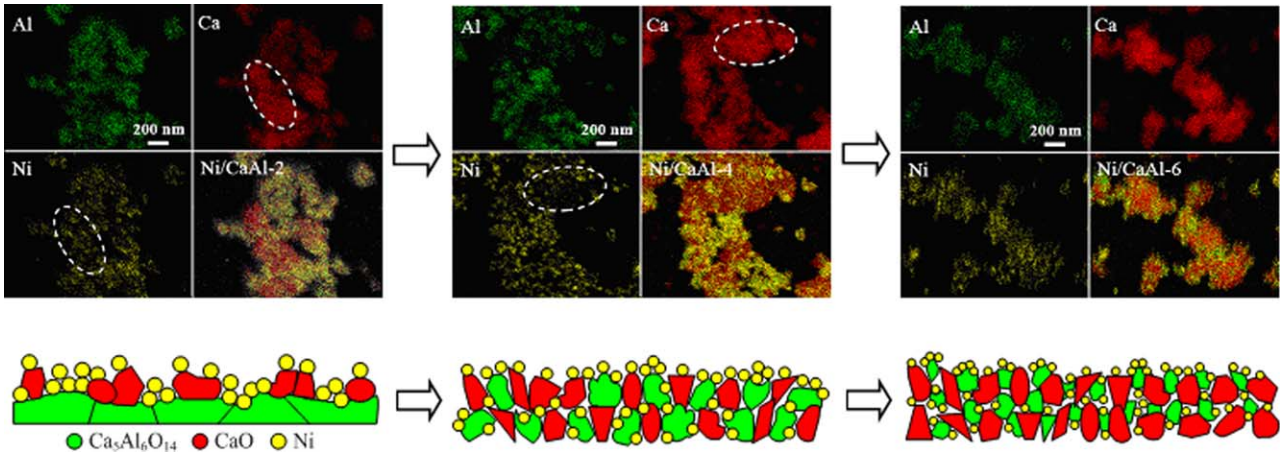

Figure 6. Structural changes of Ni/CaAl-*x* catalysts with the CaO/Al_2O_3 mass ratio.

[Color figure can be viewed in the online issue, which is available at wileyonlinelibrary.com.]

the other hand.[39] The Ni distribution in Ni/CaAl-4 becomes more uniform, but there still exists Ni-poor areas. However, for Ni/CaAl-6, neither Ca-rich nor Ni-poor areas are observed; each element is homogeneously distributed in the catalyst.

On the basis of the above characterization results, a physical model of the Ni/CaAl-*x* catalysts is proposed and illustrated in Figure 6. For Ni/CaAl-2 the distribution of $Ca_5Al_6O_{14}$ is uniform (verified by the EDS mapping of Al), but a portion of its surface is covered by CaO and in some places agglomeration of CaO occurs. As a result, the uncovered surface of $Ca_5Al_6O_{14}$ that shows a high affinity for Ni is reduced, which in turn leads to an increased amount of free NiO in the calcined catalyst (Figure 3) and subsequent larger Ni crystallites after reduction (Figure 5). For Ni/CaAl-4, both the amount and the size of $Ca_5Al_6O_{14}$ are reduced, and the distribution of CaO in the support is improved to some extent, resulting in more NiO species on the surface of $Ca_5Al_6O_{14}$ and less free NiO (Figure 3). Therefore, Ni/CaAl-4 displays relatively smaller Ni crystallites compared to Ni/CaAl-2. As for Ni/CaAl-6 or Ni/CaAl-8, both CaO and $Ca_5Al_6O_{14}$ are uniformly distributed in the support, and an optimum distribution of NiO on different sites of the support is obtained, which gives rise to the smallest Ni crystallites after reduction. When the CaO/Al_2O_3 ratio further increases, although $Ca_5Al_6O_{14}$ is well distributed in the catalyst (Supporting Information Figure S3), both the increased CaO content and the decreased $Ca_5Al_6O_{14}$ inevitably cause more NiO species on CaO and more free NiO (Figure 3), which result in relatively larger Ni crystallites after reduction in comparison with Ni/CaAl-6 and Ni/CaAl-8.

CO_2 capture capacity

Figure 7 shows the CO_2 capture capacity of various catalysts. The Ni/CaO catalyst has the highest CO_2 capture capacity (0.56 g_{CO_2}/g_{cat}) during the initial several cycles, but it drops quickly to 0.47 g_{CO_2}/g_{cat} at the 10th cycle, indicating the poor stability of Ni/CaO. On the contrary, the cyclic stability of the Ni/CaAl-*x* catalysts is significantly improved, and almost no loss-in-capacity is observed for these catalysts during 10 cycles. The good stability of Ni/CaAl-*x* is predominantly attributed to formation of $Ca_5Al_6O_{14}$ which, according to the above analyses, is uniformly distributed in the catalyst and can effectively delay sintering of CaO and $CaCO_3$ particles at high temperature. In fact, during the development of high-performance CaO-based sorbents, other calcium aluminates such as $Ca_{12}Al_{14}O_{33}$[24,56–59] and $Ca_9Al_6O_{18}$ (or $Ca_3Al_2O_6$)[43,45,60,61] have been proved to play the same role as $Ca_5Al_6O_{14}$.

It can be clearly seen that the CO_2 capture capacity of Ni/CaAl-*x* depends on the CaO/Al_2O_3 ratio. Corresponding to *x* varying from 2 to 12, the CO_2 capture capacities of these catalysts at the 10th cycle are 0.23, 0.39, 0.45, 0.49, 0.51, and 0.53 g_{CO_2}/g_{cat}, respectively. In addition, the so-called self-reactivation phenomenon,[62,63] that is, an increase in the CO_2 capture capacity during the first several cycles, is noted for almost all Ni/CaAl-*x* including Ni/CaO. The evolution of CO_2 capture capacity of Ni/CaAl-*x* with the cycling results mainly from two competing factors: increase of pore volume with the cycling (advantage) and sintering of CaO (disadvantage),[63] both of which are present for Ni/CaAl-*x*. As shown in Table 1, the pore volume of the used catalyst after 10 SESMR cycles (data in brackets) increases more or less compared to that of the fresh catalyst. Conversely, sintering of CaO with the cycling takes place, which is confirmed by

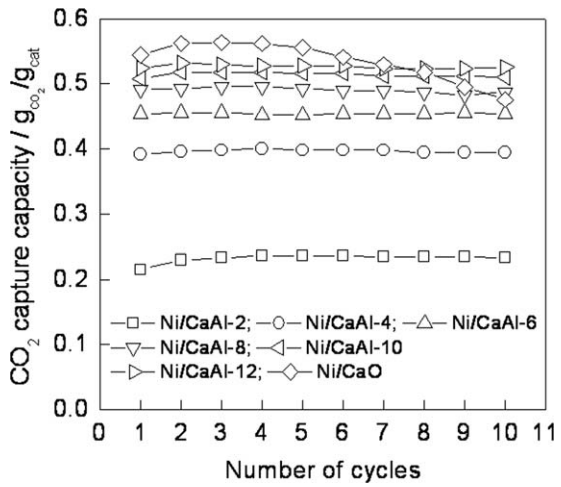

Figure 7. Comparison of the CO_2 capture capacity of various Ni/CaAl-*x* catalysts.

Carbonation: 923 K, 30 min, 15% CO_2 in N_2; calcination: 1073 K, 10 min, pure N_2; temperature ramp rate of 10 K/min.

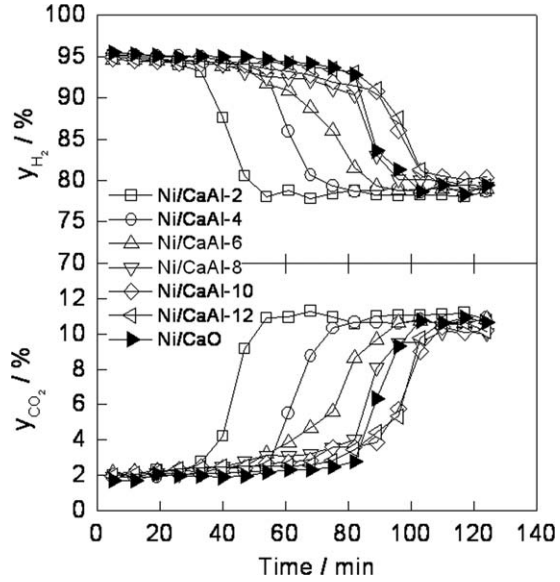

Figure 8. Comparison of the catalytic performance of various Ni/CaAl-*x* catalysts at the first cycle: catalyst (4 g), 923 K, 0.1 MPa, H_2O/CH_4 (molar ratio) = 4, $F_{CH_4,in}$ = 15.6 mL/min.

the decreased surface area (Table 1) and the increased grain size (Figure 4), especially for the catalyst with a high CaO/Al_2O_3 ratio. It should be noted from Figure 4, however, that sintering of CaO in Ni/CaAl-*x* is less severe than that in Ni/CaO, further demonstrating the contribution of $Ca_5Al_6O_{14}$ to inhibition of CaO sintering at high temperature.

Sorption-enhanced SMR

The typical profiles of molar fractions (dry basis) of various species at the outlet of the reactor are given in Supporting Information Figure S4. Three distinct regions, prebreakthrough, breakthrough, and postbreakthrough, are observed as usual.[16–21] The molar fractions of H_2, CH_4, CO, and CO_2 during the prebreakthrough period are measured to be 95.0, 0.6, 2.3, and 2.1%, respectively, which agree well with the corresponding equilibrium molar fractions (by thermodynamic calculation under the same experimental condition), being 94.5, 0.6, 2.4, and 2.5%, respectively. Likewise, the measured fractions of different species during the postbreakthrough period are close to the calculated equilibrium values. Figure 8 compares the catalytic performance of various Ni/CaAl-*x* catalysts at the first cycle to study the effect of the CaO/Al_2O_3 ratio on the SESMR process. The outlet concentration of H_2 or CO_2 during the prebreakthrough or postbreakthrough period for each catalyst is almost the same irrespective of the CaO/Al_2O_3 ratio investigated, indicating good catalytic activities of these bifunctional catalysts in SESMR, at least during the first cycle. The prebreakthrough period is observed to extend with increasing CaO/Al_2O_3 ratio from 2 to 10 and remains unchanged from 10 to 12, which coincides with the variation of the CO_2 capture capacity of Ni/CaAl-*x* with the CaO/Al_2O_3 ratio (Figure 7). It is worth noting that the prebreakthrough period of Ni/CaO is almost the same as that of Ni/CaAl-12 but its breakthrough period is shorter than that of the latter, which suggests that Ni/CaAl-12 has higher CaO utilization efficiency (or conversion) than Ni/CaO, by taking in account the higher CaO

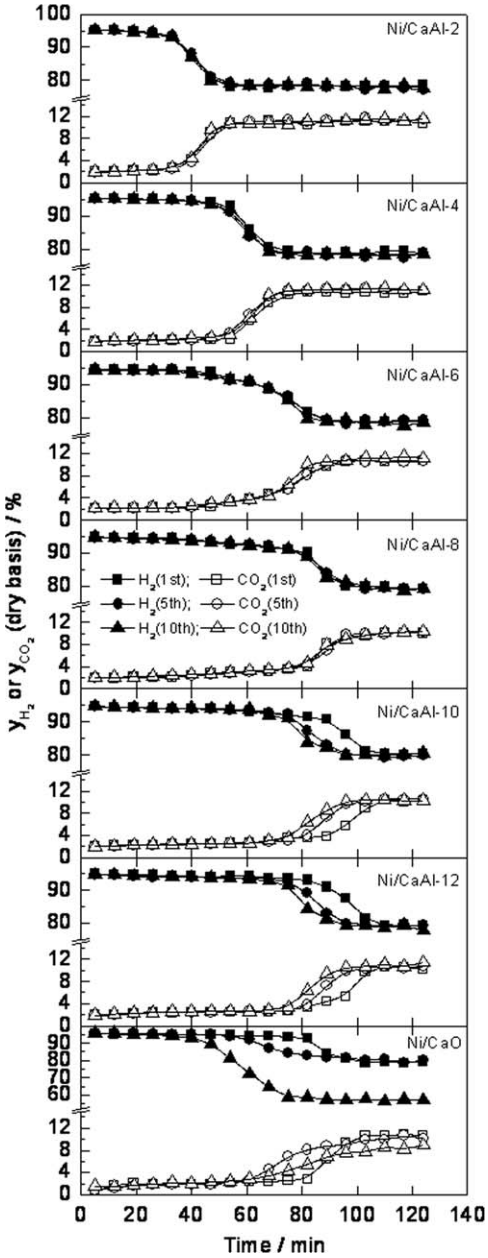

Figure 9. Comparison of the catalytic performance of various Ni/CaAl-*x* catalysts over 10 SESMR cycles: catalyst (4 g), 923 K, 0.1 MPa, H_2O/CH_4 (molar ratio) = 4, $F_{CH_4,in}$ = 15.6 mL/min.

content of Ni/CaO. Ni/CaAl-12 might have higher effective product layer diffusivity than Ni/CaO, owing to the presence of $Ca_5Al_6O_{14}$ in Ni/CaAl-12. The synthetic CaO-based sorbents do have higher effective product layer diffusivity than limestone, which has been proved in previous work.[44]

Next, the Ni/CaAl-*x* catalysts are tested over 10 consecutive SESMR cycles, and the outlet molar fraction profiles of H_2 and CO_2 at the first, fifth, and 10th cycles are presented in Figure 9. For the catalyst with a CaO/Al_2O_3 ratio no higher than 8, the H_2 or CO_2 profiles almost completely overlap, but for the catalyst with a CaO/Al_2O_3 ratio higher than 8, the profiles are different and the prebreakthrough period becomes shorter with the cycling, implying deterioration of catalyst performance. In particular, the molar fraction of H_2 in the postbreakthrough period at the 10th cycle for

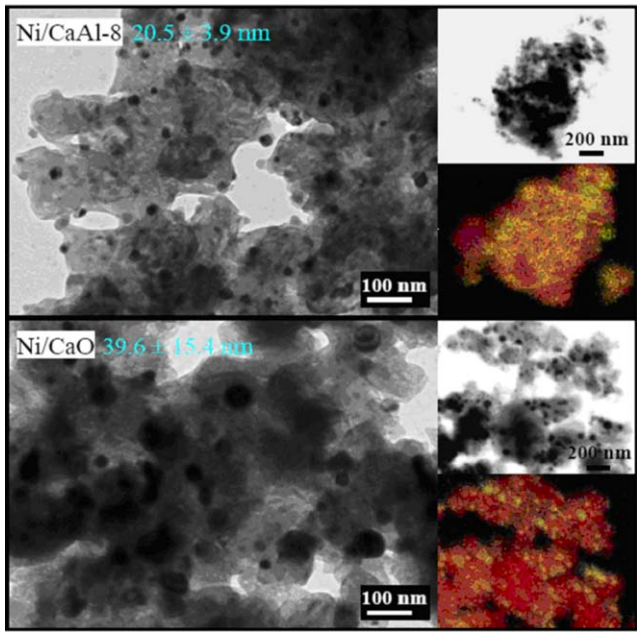

Figure 10. HRTEM images and EDS mapping of Ni/CaAl-8 and Ni/CaO catalysts after 10 SESMR cycles.

[Color figure can be viewed in the online issue, which is available at wileyonlinelibrary.com.]

Ni/CaO is only about 57%, which is much lower than the equilibrium value of 77%, indicating severe degradation of Ni/CaO. The performance degradation of Ni/CaAl-*x* with higher CaO/Al_2O_3 ratio is mainly attributed to structural changes of catalyst. As shown in Figure 4, similar to those catalysts used in TGA, the grain size of catalyst in SESMR is also found to increase after 10 cycles. Moreover, a larger increase is observed for the catalyst with a high CaO/Al_2O_3 ratio.

The XRD patterns of used catalysts after 10 SESMR cycles (Supporting Information Figure S5) demonstrate the increased crystallite size of CaO. For example, the crystallite sizes of CaO for fresh (Figure S1) and used Ni/CaAl-8 (Supporting Information Figure S5) are calculated to be 32.9 and 35.6 nm, respectively, and the corresponding values for Ni/CaO are 34.3 and 40.5 nm, respectively. It is apparent that the used Ni/CaO exhibits a larger increase in the CaO crystallite size, agreeing well with the FESEM observation (Figure 4). Another species in the catalyst support–$Ca_5Al_6O_{14}$, however, hardly varies with the cycling. For instance, the crystallite sizes of $Ca_5Al_6O_{14}$ for fresh and used Ni/CaAl-2 are 21.6 and 22.2 nm, respectively, revealing the high-thermal stability of $Ca_5Al_6O_{14}$. Compared to those of fresh catalysts, the Ni particles of used catalysts increase to some extent (Figure 10). For Ni/CaAl-8 only a small increase in the average size of Ni particles is observed (from 16.7 to 20.5 nm), but for Ni/CaO a much larger increase occurs (from 20.5 to 39.6 nm), indicating fast sintering of the Ni particles in Ni/CaO. The sintering of Ni particles is believed to be the main reason for loss of activity of Ni-based catalysts,[64,65] which explains the observed fast deactivation of Ni/CaO. On the contrary, Ni/CaAl-6 and Ni/CaAl-8 that possess uniform distribution of Ni, CaO, and $Ca_5Al_6O_{14}$, and the smallest Ni particle size among all the Ni/CaAl-*x* catalysts, show significantly increased resistance to Ni sintering during the cyclic SESMR process.

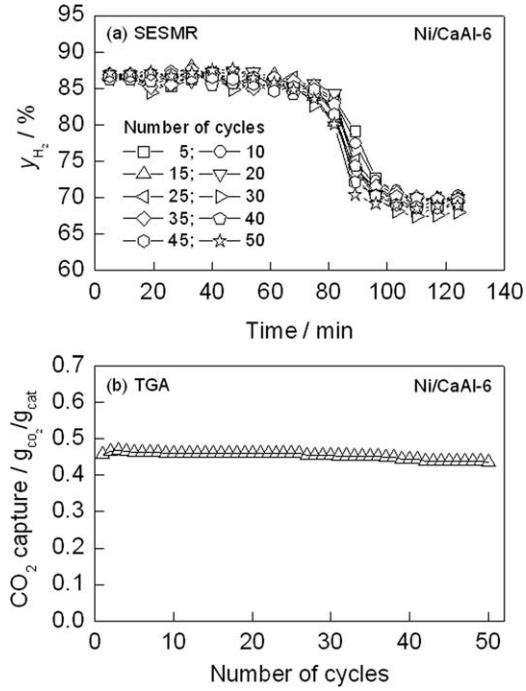

Figure 11. 50 consecutive SESMR and TGA cycles over Ni/CaAl-6: (a) SESMR: catalyst (4 g), 923 K, 0.1 MPa, H_2O/CH_4 (molar ratio) = 2, $F_{CH_4,in}$ = 15.6 mL/min; (b) TGA: carbonation: 923 K, 30 min, 15% CO_2 in N_2; calcination: 1073 K, 10 min, pure N_2; temperature ramp rate of 10 K/min.

To check the stability of the developed bifunctional catalyst in the SESMR process, Ni/CaAl-6 is further evaluated under severe conditions. 50 consecutive SESMR cycles (about 200 h) were used at a low steam/methane ratio of 2 instead of 4, which is more meaningful from economic and energy efficiency considerations.[66] As shown in Figure 11a, almost all the profiles of H_2 molar fraction during 50 cycles are identical, and the measured H_2 molar fraction during the prebreakthrough period is nearly equal to the equilibrium value (87.0%), indicating excellent activity and stability of Ni/CaAl-6. Furthermore, the measured molar fractions of CH_4, CO, and CO_2 (not shown) are close to the equilibrium values, implying that thermodynamic equilibrium is achieved under the experimental conditions.

To the best of our knowledge, previous studies[37–42,67] on bifunctional catalysts were performed at a steam/methane ratio of 3–4 and the number of SESMR cycles was no more than 30. For instance, Feng et al.[67] prepared a La_2O_3-modified Ni-CaO/Al_2O_3 catalyst, which was tested in 30 SESMR cycles with a steam/methane ratio of 4. The stability of this catalyst was well maintained for around 25 cycles, but unfortunately, it dropped for the last several cycles. The conversion of CH_4 at the 30th cycle was reduced by about 20% compared with the first cycle. In contrast, in this work the Ni/CaAl-6 catalyst is evaluated at a low steam/methane ratio of 2 over 50 cycles. Even though the operation conditions are more severe than those in previous work,[37–42,67] Ni/CaAl-6 shows high activity and stability during long-term operation, making it a high-performance bifunctional catalyst for the SESMR process.

The high stability of this catalyst is also reflected in multi-cyclic CO_2 capture operation. As displayed in Figure 11b, the CO_2 capture capacity of Ni/CaAl-6 over 50 cycles

remains almost unchanged, varying from 0.45 g_{CO_2}/g_{cat} at the first cycle to 0.44 g_{CO_2}/g_{cat} at the 50th cycle. Correspondingly, the conversion of CaO (the CaO content in Ni/CaAl-6 is 59.4 wt %) decreases slightly from 96.4 to 94.3%. In our previous study[20] on a synthetic CaO-$Ca_9Al_6O_{18}$ sorbent, the CaO conversion decreased from 92.3% at the first cycle to 77.2% at the 50th cycle under the same carbonation and calcination conditions. The improved stability of Ni/CaAl-6 is attributed to the presence of Ni species, which acts synergistically with $Ca_5Al_6O_{14}$ to inhibit the sintering of CaO.[39] Even compared with other bifunctional catalysts available in literature, Ni/CaAl-6 still exhibits high CO_2 capture performance. For example, Martavaltzi and Lemonidou[39] reported a CaO conversion of about 56% after 45 cycles for a Ni-CaO-$Ca_{12}Al_{14}O_{33}$ catalyst. Although the catalyst stability in CO_2 capture is good enough, its CaO utilization efficiency is much lower than that of Ni/CaAl-6. A Ni-Ca-based catalyst developed by Broda et al.[41] had a CaO conversion of 81% at the first cycle, but decreased to 72% at the 10th cycle.

The excellent activity and stability of Ni/CaAl-6 makes it applicable not only to the SESMR process, but also to the high-temperature CO_2 capture process, for example, capturing CO_2 from flue gases of fossil fuel-fired power plants. This catalyst may also be applied to other sorption-enhanced processes in which, for example, ethanol is used as feedstock. In addition, the sol–gel technique developed in this work can be readily extended to prepare other bifunctional catalysts, for example, Zr, Ti, and Si-stabilized Ni/CaO catalysts.

Conclusions

Ni/CaO-Al_2O_3 bifunctional catalysts were developed and applied to the SESMR process in this work. The catalysts with different CaO/Al_2O_3 mass ratios were prepared by a sol–gel method and characterized in detail by various analytic techniques. The developed catalysts were mainly composed of Ni (for reforming reaction), CaO (for CO_2 removal) and $Ca_5Al_6O_{14}$ (as support matrix), and the presence of $Ca_5Al_6O_{14}$ in the catalyst can effectively delay sintering of CaO/$CaCO_3$ at high temperature and thus improve the CO_2 capture performance. The CaO/Al_2O_3 mass ratio was found to have a significant effect on the physicochemical properties of the catalysts, such as surface area, pore volume, micromorphology, Ni particle size, element distribution, and reducibility, which in turn directly influenced the catalytic performance in SESMR. The Ni/CaO-Al_2O_3 catalyst with a CaO/Al_2O_3 mass ratio of 6 or 8 exhibited good catalytic performance over 10 consecutive SESMR cycles at 923 K and 0.1 MPa with a steam/methane molar ratio of 4, which was predominantly attributed to relatively large surface area, small Ni particle size and uniform distribution of Ni, CaO, and $Ca_5Al_6O_{14}$ in the catalyst. In particular, for the catalyst with a CaO/Al_2O_3 mass ratio of 6, both the H_2 concentration profile and the CO_2 capture capacity remained almost unchanged during 50 cycles using a low steam/methane molar ratio of 2, indicating high stability of this bifunctional catalyst in the SESMR process.

Acknowledgments

The work was supported by the National Natural Science Foundation of China (21276076), the Program for New Century Excellent Talents in University (NCET-13-0801), the Fundamental Research Funds for the Central Universities (222201313011), and the "111" project (B08021).

Literature Cited

1. International Energy Agency (IEA). *CO_2 Capture and Storage: A Key Carbon Abatement Option*. Paris: IEA Publications, 2008.
2. Wang Q, Luo JZ, Zhong ZY, Borgna A. CO_2 capture by solid adsorbents and their applications: current status and new trends. *Energy Environ Sci*. 2011;4:42–55.
3. MacDowell N, Florin N, Buchard A, Hallett J, Galindo A, Jackson G, Adjiman C. S, Williams CK, Shah N, Fennell P. An overview of CO_2 capture technologies. *Energy Environ Sci*. 2010;3:1645–1669.
4. Züttel A, Borgschulte A, Schlapbach L. *Hydrogen as a Future Energy Carrier*. Weinheim: Wiley-VCH, 2008.
5. Harrison DP. Sorption-enhanced hydrogen production: a review. *Ind Eng Chem Res*. 2008;47:6486–6501.
6. Bhat SA, Sadhukhan J. Process intensification aspects for steam methane reforming: an overview. *AIChE J*. 2009;55:408–422.
7. Tzanetis KF, Martavaltzi CS, Lemonidou AA. Comparative exergy analysis of sorption enhanced and conventional methane steam reforming. *Int J Hydrogen Energy*. 2012;37:16308–16320.
8. Connell DP, Lewandowski DA, Ramkumar S, Phalak N, Statnick RM, Fan LS. Process simulation and economic analysis of the calcium looping process (CLP) for hydrogen and electricity production from coal and natural gas. *Fuel*. 2013;105:383–396.
9. Blamey J, Anthony EJ, Wang J, Fennell PS. The calcium looping cycle for large-scale CO_2 capture. *Prog Energy Combust Sci*. 2010;36:260–279.
10. Anthony EJ. Ca looping technology: current status, developments and future directions. *Greenhouse Gas Sci Technol*. 2011;1:36–47.
11. Dean CC, Blamey J, Florin NH, Al-Jeboori MJ, Fennell PS. The calcium looping cycle for CO_2 capture from power generation, cement manufacture and hydrogen production. *Chem Eng Res Des*. 2011;89:836–855.
12. Fan LS, Zeng L, Wang W, Luo SW. Chemical looping process for CO_2 capture and carbonaceous fuel conversion—prospect and opportunity. *Energy Environ Sci*. 2012;5:7254–7280.
13. Hufton JR, Mayorga S, Sircar S. Sorption-enhanced reaction process for hydrogen production. *AIChE J*. 1999;45:248–256.
14. Ding Y, Alpay E. Adsorption-enhanced steam-methane reforming. *Chem Eng Sci*. 2000;55:3929–3940.
15. Xiu GH, Li P, Rodriguez AE. Adsorption-enhanced steam-methane reforming with intraparticle-diffusion limitations. *Chem Eng J*. 2003;95:83–93.
16. Li ZS, Cai NS. Modeling of multiple cycles for sorption enhanced steam methane reforming and sorbent regeneration in fixed bed reactor. *Energy Fuels*. 2007;21:2909–2918.
17. Martavaltzi CS, Pampaka EP, Korkakaki ES, Lemonidou AA. Hydrogen production via steam reforming of methane with simultaneous CO_2 capture over CaO-$Ca_{12}Al_{14}O_{33}$. *Energy Fuels*. 2010;24:2589–2595.
18. Sultana KS, Chen D. Enhanced hydrogen production by in situ CO_2 removal on CaCeZrOx nanocrystals. *Catal Today*. 2011;171:43–51.
19. Ramkumar S, Phalak N, Fan LS. Calcium looping process (CLP) for enhanced steam methane reforming. *Ind Eng Chem Res*. 2012;51:1186–1192.
20. Xie MM, Zhou ZM, Qi Y, Cheng ZM, Yuan WK. Sorption-enhanced steam methane reforming by in situ CO_2 capture on a CaO-$Ca_9Al_6O_{18}$ sorbent. *Chem Eng J*. 2012;207–208:142–150.
21. Broda M, Manovic V, Imtiaz Q, Kierzkowska AM, Anthony EJ, Müller CR. High-purity hydrogen via the sorption-enhanced steam methane reforming reaction over a synthetic CaO-based sorbent and a Ni catalyst. *Environ Sci Technol*. 2013;47:6007–6014.
22. Feng B, An H, Tan E. Screening of CO_2 adsorption materials for zero emission power generation systems. *Energy Fuels*. 2007;21:426–434.
23. Ochoa-Fernández E, Haugen G, Zhao TJ, Rønning M, Aartun I, Børresen B, Rytter E, Rønnekleiv M, Chen D. Process design simulation of H2 production by sorption enhanced steam methane reforming: evaluation of potential CO_2 acceptors. *Green Chem*. 2007;9:654–662.
24. Koirala R, Reddy GK, Smirniotis PG. Single nozzle flame-made highly durable metal doped Ca-based sorbents for CO_2 capture at high temperature. *Energy Fuels*. 2012;26:3103–3109.

25. Wang SP, Yan SL, Ma XB, Gong JL. Recent advances in capture of carbon dioxide using alkali-metal-based oxides. *Energy Environ Sci*. 2011;4:3805–3819.
26. Yu FC, Phalak N, Sun ZC, Fan LS. Activation strategies for calcium-based sorbents for CO_2 capture: a perspective. *Ind Eng Chem Res*. 2012;51:2133–2142.
27. Liu WQ, An H, Qin CL, Yin JJ, Wang GX, Feng B, Xu MH. Performance enhancement of calcium sorbents for cyclic CO_2 capture—a review. *Energy Fuels*. 2012;26:2751–2767.
28. Valverde JM. Ca-based synthetic materials with enhanced CO_2 capture efficiency. *J Mater Chem A*. 2013;1:447–468.
29. Kierzkowska AM, Pacciani R, Müller CR. CaO-based CO_2 sorbents: from fundamentals to the development of new, highly effective materials. *ChemSusChem*. 2013;6:1130–1148.
30. Grünewald M, Agar DW. Enhanced catalyst performance using integrated structured functionalities. *Chem Eng Sci*. 2004;59:5519–5526.
31. Dietrich W, Lawrence PS, Grünewald M, Agar DW. Theoretical studies on multifunctional catalyst with integrated adsorption sites. *Chem Eng J*. 2005;107:103–111.
32. Lawrence PS, Grünewald M, Agar DW. Spatial distribution of functionalities in an adsorptive reactor at the particle level. *Catal Today*. 2005;105:582–588.
33. Kapil A, Bhat SA, Sadhukhan J. Multiscale characterization framework for sorption enhanced reaction processes. *AIChE J*. 2008;54:1025–1036.
34. Solsvik J, Jakobsen HA. A numerical study of a two property catalyst/sorbent pellet design for the sorption-enhanced steam-methane reforming process: modeling complexity and parameter sensitivity study. *Chem Eng J*. 2011;178:407–422.
35. Rout KR, Solsvik J, Nayak AK, Jakobsen HA. A numerical study of multicomponent mass diffusion and convection in porous pellets for the sorption-enhanced steam methane reforming and desorption processes. *Chem Eng Sci*. 2011;66:4111–4126.
36. Rout KR, Jakobsen HA. A numerical study of pellets having both catalytic- and capture properties for SE-SMR process: kinetic- and product layer diffusion controlled regimes. *Fuel Process Technol*. 2013;106:231–246.
37. Satrio JA, Shanks BH, Wheelock TD. Development of a novel combined catalyst and sorbent for hydrocarbon reforming. *Ind Eng Chem Res*. 2005;44:3901–3911.
38. Albrecht KO, Satrio JA, Shanks BH, Wheelock TD. Application of a combined catalyst and sorbent for steam reforming of methane. *Ind Eng Chem Res*. 2010;49:4091–4098.
39. Martavaltzi CS, Lemonidou AA. Hydrogen production via sorption enhanced reforming of methane: development of a novel hybrid material–reforming catalyst and CO_2 sorbent. *Chem Eng Sci*. 2010;65:4134–4140.
40. Chanburanasiri N, Ribeiro AM, Rodrigues AE, Arpornwichanop A, Laosiripojana N, Praserthdam P, Assabumrungrat S. Hydrogen production via sorption enhanced steam methane reforming process using Ni/CaO multifunctional catalyst. *Ind Eng Chem Res*. 2011;50:13662–13671.
41. Broda M, Kierzkowska AM, Baudouin D, Imtiaz Q, Copéret C, Müller CR. Sorbent-enhanced methane reforming over a Ni-Ca-based, bifunctional catalyst sorbent. *ACS catal*. 2012;2:1635–1646.
42. Kim JN, Ko CH, Yi KB. Sorption enhanced hydrogen production using one-body CaO-$Ca_{12}Al_{14}O_{33}$-Ni composite as catalytic absorbent. *Int J Hydrogen Energy*. 2013;38:6072–6078.
43. Zhou ZM, Qi Y, Xie MM, Cheng ZM, Yuan WK. Synthesis of CaO-based sorbents through incorporation of alumina/aluminate and their CO_2 capture performance. *Chem Eng Sci*. 2012;74:172–180.
44. Zhou ZM, Xu P, Xie MM, Cheng ZM, Yuan WK. Modeling of the carbonation kinetics of a synthetic CaO-based sorbent. *Chem Eng Sci*. 2013;95:283–290.
45. Xu P, Xie MM, Cheng ZM, Zhou ZM. CO_2 capture performance of CaO-based sorbents prepared by a sol-gel method. *Ind Eng Chem Res*. 2013;52:12161–12169.
46. Ropp RC. *Encyclopedia of the Alkaline Earth Compounds*. Amsterdam: Elsevier, 2013.
47. Mastin J, Aranda A, Meyer J. New synthesis method for CaO-based synthetic sorbents with enhanced properties for high-temperature CO_2-capture. *Energy Proced*. 2011;4:1184–1191.
48. Wu GW, Zhang CX, Li SR, Huang ZQ, Yan S, Wang SP, Ma XB, Gong JL. Sorption enhanced steam reforming of ethanol on Ni-CaO-Al_2O_3 multifunctional catalysts derived from hydrotalcite-like compounds. *Energy Environ Sci*. 2012;5:8942–8949.
49. Busca G. The surface of transitional aluminas: a critical review. *Catal Today*. 2014;226:2–13.
50. Alphonse P, Courty M. Structural and thermal behavior of nanocrystalline boehmite. *Thermochim Acta*. 2005;425:75–89.
51. Douy A, Gervais M. Crystallization of amorphous precursors in the calcia-alumina system: a differential scanning calorimetry study. *J Am Ceram Soc*. 2000;83:70–76.
52. Vella LD, Specchia S. Alumina-supported nickel catalysts for catalytic partial oxidation of methane in short-contact time reactors. *Catal Today*. 2011;176:340–346.
53. Zangouei M, Moghaddam AZ, Arasteh M. Then influence of nickel loading on reducibility of NiO/Al_2O_3 catalysts synthesized by sol-gel method. *Chem Eng Res Bull*. 2010;14:97–102.
54. Jiménez-González C, Boukha Z, Rivas BDe, Delgado JJ, Cauqui MÁ, J. R. González-Velasco, Gutiérrez-Ortiz JI, López-Fonseca R. Structural characterisation of Ni/alumina reforming catalysts activated at high temperatures. *Appl Catal A: Gen*. 2013;466:9–20.
55. Lu H, Khan A, Pratsinis SE, Smirniotis PG. Flame-made durable doped-CaO nanosorbents for CO_2 capture. *Energy Fuels*. 2009,23:1093–1100.
56. Li ZS, Cai NS, huang YY, Han HJ. Synthesis, experimental studies, and analysis of a new calcium-based carbon dioxide absorbent. *Energy Fuels*. 2005;19:1447–1452.
57. Manovic V, Anthony EJ. CaO-based pellets supported by calcium aluminate cements for high-temperature CO_2 capture. *Environ Sci Technol*. 2009;43:7117–7122.
58. Florin NH, Blamey J, Fennell PS. Synthetic CaO-based sorbent for CO_2 capture from large-point sources. *Energy Fuels*. 2010;24:4598–4604.
59. Li ZS, Liu Y, Cai NS. Understanding the effect of inert support on the reactivity stabilization for synthetic calcium based sorbents. *Chem Eng Sci*. 2013;89:235–243.
60. Liu WQ, Feng B, Wu YQ, Wang GX, Barry J, Diniz Da Costa JC. Synthesis of sintering-resistant sorbents for CO_2 capture. *Environ Sci Technol*. 2010;44:3093–3097.
61. Zhang MM, Peng YX, Sun YZ, Li P, Yu JG. Preparation of CaO-Al_2O_3 sorbent and CO_2 capture performance at high temperature. *Fuel*. 2013;111:636–642.
62. Manovic V, Anthony EJ. Thermal activation of CaO-based sorbent and self-reactivation during CO_2 capture looping cycles. *Environ Sci Technol*. 2008;42:4170–4174.
63. Stendardo S, Andersen LK, Herce C. Self-activation and effect of regeneration conditions in CO_2-carbonation looping with CaO-$Ca_{12}Al_{14}O_{33}$ sorbent. *Chem Eng J*. 2013;220:383–394.
64. Sehested J. Sintering of nickel steam-reforming catalysts. *J Catal*. 2003;217:417–426.
65. Sehested J, Gelten JAP, Remediakis IN, Bengaard H, Nørskov JK. Sintering of nickel steam-reforming catalysts: effects of temperature and steam and hydrogen pressures. *J Catal*. 2004;223:432–443.
66. Rostrup-Nielsen JR. Steam reforming. In: Ertl G, Knözinger H, Schüth F, Weitkamp J. *Handbook of Heterogeneous Catalysis*, 2nd ed. Weinheim: Wiley-VCH, 2008:2882–905.
67. Feng HZ, Lan PQ, Wu SF. A study on the stability of a NiO-CaO/Al_2O_3 complex catalyst by La_2O_3 modification for hydrogen production. *Int J Hydrogen Energy*. 2012;37:14161–14166.

Manuscript received Oct. 20, 2013, and revision received June 24, 2014.